Theoretical and experimental study of plasmonic effects in heavily doped gallium arsenide and indium phosphide

M. Cada,[1,2,*] D. Blazek,[1,2] J. Pistora,[2] K. Postava,[2] and P. Siroky[2]

[1]*Department of Electrical and Computer Engineering, Dalhousie University, Halifax, B3J 2X4 Nova Scotia, Canada*
[2]*Nanotechnology Centre, VSB-Technical University of Ostrava, 17. listopadu 15, Ostrava-Poruba, 708 33, Czech Republic*
*michael.cada@dal.ca

Abstract: Dispersion plasmonic interaction at an interface between a doped semiconductor and a dielectric is employed to use experimental data for determining the plasma frequency, the relaxation time, the effective mass, and the mobility of free electrons in heavily donor-doped gallium arsenide (GaAs) and indium phosphide (InP). A new solution for a plasmonic resonance at a semiconductor/dielectric interface found recently is exploited advantageously when analyzing the experimental data. Two independent measurement methods were used, namely the infrared reflectivity and the Raman scattering. Results indicate a good agreement with known data while pointing to some inaccuracies reported, and suggest a new alternative and accurate means to determine these important semiconductor parameters.

OCIS codes: (190.3270) Nonlinear optics, Kerr effect, (230.4320l), Nonlinear optical devices.

References and links

1. H. Raether, *Surface Plasmons on Smooth and Rough Surfaces* (Springer - Verlag, 1986).
2. S. A. Maier, *Plasmonics Fundamentals and Applications* (Springer Science + Business Media LLC, 2007).
3. P. Berini, "Bulk and surface sensitivities of surface plasmon waveguides," New J. Phys. **10**(10), 105010 (2008).
4. I. De Leon and P. Berini, "Amplification of long-range surface plasmons by a dipolar gain medium," Nat. Photonics **4**(6), 382–387 (2010).
5. M. Cada, The Institute of Photonic Sciences (ICFO), Mediterranean Technology Park, 3 Av. Carl Friedrich Gauss, 08860 Castelldefels - Barcelona, Spain (research report, 2008).
6. T. Wijesinghe, M. Premaratne, and G. P. Agrawal, "Electrically pumped hybrid plasmonic waveguide," Opt. Express **22**(3), 2681–2694 (2014).
7. J. W. Cleary, R. E. Peale, D. J. Shelton, G. D. Boreman, C. W. Smith, M. Ishigami, R. Soref, A. Drehman, and W. R. Buchwald, "IR permittivities for silicides and doped silicon," J. Opt. Soc. Am. B **27**(4), 730–734 (2010).
8. D. Li and C. Z. Ning, "All-semiconductor active plasmonic system in mid-infrared wavelengths," Opt. Express **19**(15), 14594–14603 (2011).
9. M. Cada and J. Pistora, "Optical plasmons in semiconductors," in *Proceedings of 13th International Symposium on Microwave and Optical Technology ISMOT 2011*, Prague, Czech Republic, 20–23 June 2011.
10. J. Yuan, B. Chen, and A. L. Holmes, Jr., "Improved quantum efficiency of InGaAs/InP photodetectors using Ti/Au-SiO_2 phase-matched-layer reflector," Electron. Lett. **48**(19), 1230–1232 (2012).
11. I. Kimukin, N. Biyikli, B. Butun, O. Aytur, S. M. Ünlü, and E. Ozbay, "InGaAs-Based High-Performance p-i-n Photodiodes," IEEE Photon. Technol. Lett. **14**(3), 366–368 (2002).
12. B. Chen and A. L. Holmes, Jr., "Optical gain modeling of InP based InGaAs(N)/GaAsSb type-II quantum wells laser for mid-infrared emission," Opt. Quantum Electron. **45**(2), 127–134 (2013).
13. P. Yu and M. Cardona, *Fundamentals of Semiconductors: Physics and Material Properties* (Springer, 2010).
14. W. K. Metzger, M. W. Wanlass, L. M. Gedvilas, J. C. Verley, J. J. Carapella, and R. K. Ahrenkiel, "Effective electron mass and plasma filter characterization of n-type InGaAs and InAsP," J. Appl. Phys. **92**(7), 3524–3529 (2002).
15. C. Hamaguchi, *Basic Semiconductor Physics* (Springer-Verlag, 2010).
16. M. Fox, *Optical Properties of Solids*, (Oxford University Press, 2012).
17. C. J. Johnson, G. H. Sherman, and R. Weil, "Far infrared measurement of the dielectric properties of GaAs and CdTe at 300K and 8K," Appl. Opt. **8**(8), 1667–1671 (1969).

#224420 - $15.00 USD Received 9 Oct 2014; revised 12 Dec 2014; accepted 21 Dec 2014; published 13 Jan 2015

18. M. B. Kagan, M. M. Koltun, and A. P. Landsman, "Investigation of the reflectivity of highly doped gallium arsenide in a wide spectral range," J. Appl. Spectrosc. **5**(6), 548–550 (1966).
19. M. J. Weber, *Handbook of Optical Materials* (CRC Press, 2002).
20. E. D. Palik, *Handbook of Optical Constants of Solids (*Academic Press, 1985).
21. M. Miyao, T. Motooka, N. Tatsuaki, and T. Tokuyama, "Change of the electron effective mass in extremely heavily doped n-type Si obtained by ion implantation and laser annealing," Solid State Commun. **37**(7), 605–608 (1981).
22. D. M. Szmyd, P. Porro, A. Majerfeld, and S. Lagomarsino, "Heavily doped GaAs:Se. I. Photoluminescence determination of the electron effective mass," J. Appl. Phys. **68**(5), 2367–2375 (1990).
23. D. Schneider, D. Rurup, A. Plichta, H. U. Grubert, A. Schlachetzki, and K. Hansen, "Shubnikov-de Haas effect and effective mass in n-InP in dependence on carrier concentration," Z. Phys. B. **95**, 281–285 (1994).

1. Introduction

Optical plasmons have been studied for many years [1]. The original gas plasmonic effects gave rise to interest in establishing similar electron gas collective oscillations in solid state materials. Metals are the first obvious choice as their high free electron concentrations lend themselves to such resonances. The metal electron gas can be viewed as a charged liquid of sorts and as such it displays, under certain conditions, an electromagnetic-wave-supporting characteristic.

Intense research over the last decades yielded a number of interesting results as well as applications [2]. Metals such as silver have shown to support strong plasmonic oscillations at optical frequencies along an interface with air or a dielectric. Already successfully developed applications include biological or chemical sensors [3], or waveguide-based optical structures and devices [4]. A potential exists in exploiting the surface plasmonic resonances for developing loss compensating or light amplifying devices [5, 6].

Semiconductors have been studied up until now for surface plasmons at millimeter waves (terahertz frequencies). Recent interest in finding materials [7] and methods [8] to generate optical plasmonic effects in semiconductors has been quite promising. A thorough theoretical treatment of a plasmonic interaction at an interface between a doped semiconductor and a dielectric was developed in [9]. A new solution to a complete dispersion equation under such conditions was found. Since a semiconductor material can possess a higher background permittivity than that of the interfacing dielectric, the dispersion equation acquires a third solution, in addition to the well-known surface plasmonic and the bulk branches. Such a situation cannot occur with a metal/dielectric configuration since the metal permittivity equals to the permittivity of vacuum. Therefore the new solution mentioned does not exist in the metal-based structures.

Determining important semiconductor material parameters such as permittivity, effective mass, plasma frequency, relaxation time, or mobility is crucial for proper modelling and design of semiconductor devices. For example in advanced photodetectors [10, 11] or quantum well lasers [12] the application parameters such as quantum efficiency or optical gain can be well understood and significantly improved as a result of knowing the basic material properties.

The infrared reflectivity measurement and Raman scattering are well established methods [13] and were used in similar experiments [14]. Their use in this work is a novel approach in that it combines the experimental data obtained from both independent methods with a new theoretical result in a unique way that enables one to determine the above mentioned important semiconductor parameters accurately and reliably.

2. Theory

The well-known Drude model used for metals when studying surface plasmons can be employed to describe behavior of carriers in heavily doped semiconductors [15]. Two modifications need to be made to properly address the difference between metals and semiconductors. First, the mass of a free-like electron in metal has to be characterized by an effective mass, m^*, of a carrier (electron or hole) in a semiconductor. Second, the lattice

#224420 - $15.00 USD Received 9 Oct 2014; revised 12 Dec 2014; accepted 21 Dec 2014; published 13 Jan 2015

permittivity of a semiconductor is high regardless of the concentration of carriers; only when the concentration is very high, close to the levels of metals, it can be assumed that it effectively screens the polarization of the lattice, as it is discussed in [7].

In the cases studied here, however, such a situation does not occur since the electron concentration levels of our samples are still at least two to three orders of magnitude lower than those in metals. Therefore the semiconductor's background polarizability must be accounted for by considering the semiconductor crystal lattice permittivity, ε_S, corresponding to the value when free carriers are not present [16]. The permittivity in the doped semiconductor, ε_{DS}, is thus described by the Drude model as:

$$\varepsilon_{DS} = \varepsilon_S - \frac{\tilde{\omega}_p^2}{\omega^2 + i\gamma\omega} \approx \varepsilon_S - \frac{\tilde{\omega}_p^2}{\omega^2}. \tag{1}$$

In the wavelength region of interest, both materials considered here – GaAs and InP – are completely transparent. It is usually assumed [11] that both material systems are lightly damped and thus the damping term in the Drude model above – described by the imaginary part – is ignored as indicated in Eq. (1). For the cases here, however, the free carrier damping effects are considered as explained later. In Eq. (1), ω is the light frequency, and γ is free electron damping. It depends indirectly on the free electron concentration, *N*, via the effective mass, m^*, and the mobility, μ:

$$\gamma = \frac{e}{m_0 m^* \mu} = \frac{1}{\tau}. \tag{2}$$

where m_0 is the mass of a free electron, *e* is the electron charge, and τ is the relaxation time. The parameter $\tilde{\omega}_p$, called here the Drude frequency, is related to the free electron concentration and the effective mass as:

$$\tilde{\omega}_p = \hbar\sqrt{\frac{N}{m_0 \varepsilon_0 m^*}}\ [eV]. \tag{3}$$

where ε_0 is the permittivity of vacuum and $\hbar = h/2\pi$ with *h* being the Planck's constant.

ε_S in Eq. (1) is the material's background dispersive permittivity that is evaluated by adding ionic or lattice contributions, such as optical phonons for example, to the undispersed lattice permittivity base. In the wavelength region where our reflectivity measurements were conducted, it is the transverse optical lattice vibrational mode – optical phonon (TO) – that affects its value. Its real part can be described by [17]:

$$\varepsilon_S = \varepsilon_\infty + \left(\varepsilon_{DC} - \varepsilon_\infty\right)\left[1 - \kappa^2 + \frac{\kappa^2\rho^2}{1-\kappa^2}\right]^{-1}. \tag{4}$$

where ε_{DC} is the material static permittivity, ε_∞ is the material high-frequency permittivity, $\kappa = \omega/\omega_{TO}$, ω_{TO} is the transverse optical phonon frequency, and $\rho = \gamma_{TO}/\omega_{TO}$ is a unit-less damping factor with γ_{TO} being phonon damping. $\rho \le 0.01$ for both undoped GaAs and InP, and thus can be neglected. The effect of free carriers on phonon damping, which we evaluated as 0.0089 for GaAs and 0.0066 for InP, is thus also negligible since it yields values less than 0.01 for both doped GaAs and InP studied here. For the purposes of the work presented here, other effects such as intervalence band absorption (only p-type semiconductor) and impurity absorption are not considered or neglected. Details related to these issues are found in [16].

#224420 - $15.00 USD Received 9 Oct 2014; revised 12 Dec 2014; accepted 21 Dec 2014; published 13 Jan 2015

Accounting for the semiconductor's background polarizability by including the crystal lattice permittivity, ε_S, modifies the Drude frequency, $\tilde{\omega}_p$, into a form used in literature and called the plasma frequency, ω_p, of a semiconductor material that possesses a high lattice permittivity[10]. For cases when the dopants concentration is high enough, a usual and convenient approximation is made whereby ε_S is replaced with ε_∞ and the plasma frequency is defined as:

$$\omega_p = \hbar\sqrt{\frac{N}{m_0\varepsilon_0\, m^*\varepsilon_\infty}}\ [eV]. \tag{5}$$

which is valid when $\omega_p \gg \omega_{TO}$. If the plasma frequency is far below the optical phonon frequency, the permittivity ε_∞ in Eq. (5) should be replaced with ε_{DC}. It can be noticed from Eqs. (3) and (5) that the relationship between the Drude frequency $\tilde{\omega}_p$ and the plasma frequency ω_p is simply:

$$\omega_p = \frac{\tilde{\omega}_p}{\sqrt{\varepsilon_\infty}}\,. \tag{6}$$

The value of the plasma frequency can be obtained from the Raman scattering measurements. The Raman scattering trace does not yield directly the plasma frequency since it is a coupled mode of the plasma oscillations with the longitudinal optical (LO) phonon that produces the Raman shift. Its dependence on the carrier concentration is crucial to recognize and include in the analysis of experimental data. It is this concentration dependence of the plasmon/phonon coupled mode that yields the free electron plasma frequency in the case of heavy doping of the samples studied. A theoretical model described in [15] is applicable to the cases investigated here. The Raman shift, $\omega_\pm$, is given by:

$$\omega_\pm^2 == \frac{1}{2}\left(\omega_{LO}^2 + \omega_p^2 + \gamma_{TO}\,\gamma\right) \pm \frac{1}{2}\sqrt{\left(\omega_{LO}^2 + \omega_p^2 + \gamma_{TO}\,\gamma\right)^2 - 4\,\omega_p^2\,\omega_{TO}^2}\,. \tag{7}$$

where ω_{LO} is the longitudinal optical phonon frequency. It can be noted that the measured ω_+ equals simply to $\tilde{\omega}_p / \sqrt{\varepsilon_S}$.

We now consider a semiconductor/dielectric interface and assume a surface plasmon TM-polarized electric field propagating along the z-axis and decaying exponentially away (x-axis) from both sides of the interface as follows:

$$\begin{aligned} E_{x,z} &= E_{x,z}^{D,S}\,\delta_{D,S} \\ \delta_{D,S} &= e^{-i\omega t} e^{i\psi_{D,S}\,x} e^{i\beta z}. \end{aligned} \tag{8}$$

where $\psi_{D,S}$ and β are the transversal and longitudinal propagation constants, respectively. Subscripts *S* and *D* refer to the semiconductor and dielectric, respectively. Satisfying the relevant boundary conditions for electric and magnetic fields leads to the complete dispersion equation in the form [9]:

$$\left(\varepsilon_S - \varepsilon_D\right)\omega^6 + \left[\left(\frac{\varepsilon_D}{\varepsilon_S} - 2\right)\tilde{\omega}_p^2 + \left(\frac{\varepsilon_D}{\varepsilon_S} - \frac{\varepsilon_S}{\varepsilon_D}\right)\beta^2 c^2\right]\omega^4 + \frac{1}{\varepsilon_S}\left(\tilde{\omega}_p^2 + 2\frac{\varepsilon_S}{\varepsilon_D}\beta^2 c^2\right)\tilde{\omega}_p^2\,\omega^2 - \frac{1}{\varepsilon_S\,\varepsilon_D}\tilde{\omega}_p^4\,\beta^2 c^2 = 0 \tag{9}$$

#224420 - $15.00 USD Received 9 Oct 2014; revised 12 Dec 2014; accepted 21 Dec 2014; published 13 Jan 2015

where ε_D is the permittivity of the interfacing dielectric medium, and c is the speed of light in vacuum. Equation (9) possesses three independent solutions. Two are the known solutions for the surface plasmon and the free electron dispersion in bulk. For the case studied here when $\varepsilon_S > \varepsilon_D$ Eq. (9) also indicates another real solution (which corresponds actually to the case when $\varepsilon_{DS} = \varepsilon_D$) that does not exist in the metal-based structures. It can be shown that the solution is a constant with respect to β:

$$\omega_{op}^2 = \frac{\tilde{\omega}_p^2}{\varepsilon_S - \varepsilon_D}. \tag{10}$$

The solution in Eq. (10) exists only when $\varepsilon_S > \varepsilon_D$, which explains why it cannot appear in the metal since it would mean an imaginary frequency. Figure 1 shows all three solutions. The straight line (thin red) is the light line, the curve above it (green) is the bulk dispersion of free electrons with the value of $\tilde{\omega}_p / \sqrt{\varepsilon_S}$ at $\beta = 0$, the curve below it (blue) is the surface plasmon dispersion with the asymptotic value of $\tilde{\omega}_p / \sqrt{\varepsilon_S + \varepsilon_D}$ at $\beta = \infty$, and the red horizontal line is the solution in Eq. (10). As can be realized, its position can be varied by the choice of the interfacing dielectric. This is illustrated by the experimental data in the next section. InP sample parameters and air were used for this figure.

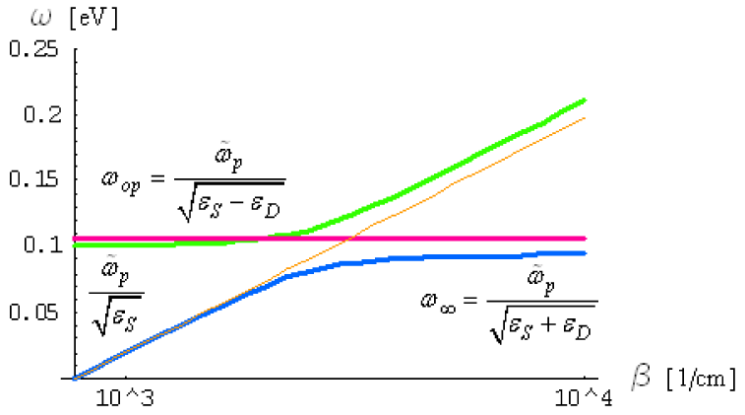

Fig. 1. Dispersion of semiconductor/dielectric interface.

It can be inferred from Fig. 1 that the reflectivity of an interface possesses a minimum at the frequency ω_{op}. Its value can thus be obtained from infrared reflectivity measurements. The plasma frequency in doped semiconductors where concentrations of electrons are much smaller than those in metals lies in the infrared spectral range. The infrared reflectivity spectrum of doped semiconductors is basically featureless within that range, thus the plasma edge shows up as very well defined. The fundamental absorption edge and the phonon absorption bands are well away from it, therefore a distinct minimum peak corresponding to the plasmon energy is easily observable and distinguishable [18]. As explained in the following section, the dispersion of ε_S must be considered in order to correctly interpret measured data.

The minimum of the reflectivity reaches a zero value at the frequency ω_{op} when free electron damping is negligibly small. On the other hand, the damping factor γ can, in turn, be determined from the minimum reflectivity $R_{\min}$ measured at the single interface (air/semiconductor) with a near-normal light beam incident from the air. Using the Fresnel

#224420 - $15.00 USD Received 9 Oct 2014; revised 12 Dec 2014; accepted 21 Dec 2014; published 13 Jan 2015

reflection coefficient one can find a position of the minimum by evaluating the first derivative of the reflectivity with respect to the frequency. The exact implicit solution has the form $\Re\left\{\sqrt{\varepsilon_{DS}}\left(\varepsilon_{DS}-1\right)\frac{d\varepsilon_{DS}^{*}}{d\omega}\right\}$ where $\Re$ is the real part and the asterisk represents a complex conjugated number. The explicit solution can be found by an approximation that the derivative of the imaginary part of the permittivity is negligible compared to the derivative of the real part of the permittivity near the reflectivity minimum. Substituting the obtained solution back to the Fresnel equation one obtains an approximate solution:

$$\gamma=\frac{\omega_{op}^{3}}{\tilde{\omega}_{p}^{2}}\frac{4\sqrt{R_{\min}}\left(1+R_{\min}\right)}{\left(1-R_{\min}\right)^{2}}. \tag{11}$$

Determining γ from Eq. (11) yields directly the relaxation time τ in Eq. (2). It is interesting to note that by freely choosing the permittivity of the interfacing medium, ε_{D}, one can move ω_{op} basically arbitrarily to higher frequencies, theoretically even up to the visible range. This feature is demonstrated experimentally in the following section.

3. Experiment

Two types of samples were studied experimentally; a heavily doped n-type GaAs and a heavily doped n-type InP. Two independent measurement methods were employed, namely the infrared reflectivity and the Raman scattering measurements were performed to obtain desired materials parameters. Table 1 gives basic parameters of the samples studied.

Table 1. Given parameters

Parameter/Material	GaAs	InP
concentration, N $[cm^{-3}]$	2.4×10^{18}	1.0×10^{19}
high frequency permittivity, ε_{∞}	10.9	9.6
static permittivity, ε_{DC}	12.8	12.5
interface permittivity, ε_{D}	1 or 5.66	1 or 5.66
TO phonon energy, ω_{TO} $[cm^{-1}]$	269	304
LO phonon energy, ω_{LO} $[cm^{-1}]$	292	345
phonon damping factor, ρ	≤ 0.01	≤ 0.01

Infrared reflectivity

The reflectivity was obtained using Fourier Transform InfraRed (FTIR) spectrometer Vertex 70v from Bruker, for mid and far infrared spectral ranges, with standard Globar source, room temperature DlaTGS detectors, and mid-infrared KBr and far-infrared Mylar beamsplitters. Examples of the infrared reflectivity spectrum of GaAs and InP samples are shown in Figs. 2 and 3, respectively. The spectra are shown as a function of the wavenumber. Two curves are shown in each figure. They represent two measurements on the same sample but with a different interfacing dielectric. The red curve corresponds to air with the incident light beam being near-normal to the surface with an angle of incidence of 11 degree. The spectrum was normalized using the reflectivity measurement from a gold reference.

The blue line corresponds to diamond with an incident light beam being at 45 degrees with respect to the surface. The minima observed, called here the plasma edge, correspond to the new plasmonic mode predicted theoretically [9] and shown in Eq. (10) above. Both minima are clearly seen in both cases. The shift in the minimum with a change in the

#224420 - $15.00 USD Received 9 Oct 2014; revised 12 Dec 2014; accepted 21 Dec 2014; published 13 Jan 2015

interfacing dielectric is a direct consequence of Eq. (10). Since the height of the minimum indicates the amount of damping as per Eq. (11), the imaginary part of the semiconductor permittivity, ε_{DS} in Eq. (1), decreases with increasing the frequency, which is clearly shown in both figures when one compares minima for air and diamond interfaces.

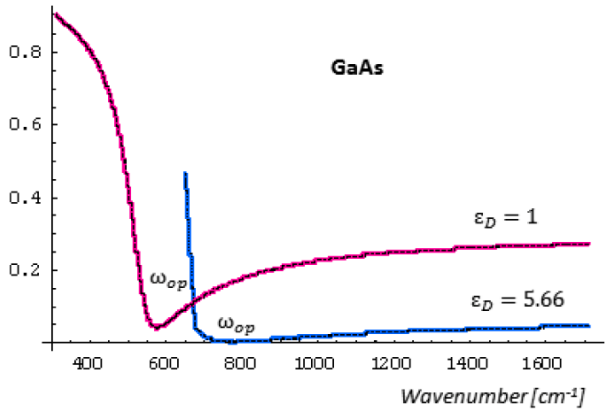

Fig. 2. Reflectivity spectrum of a heavily doped n-type GaAs: red curve – GaAs/air interface, blue curve – GaAs/diamond interface.

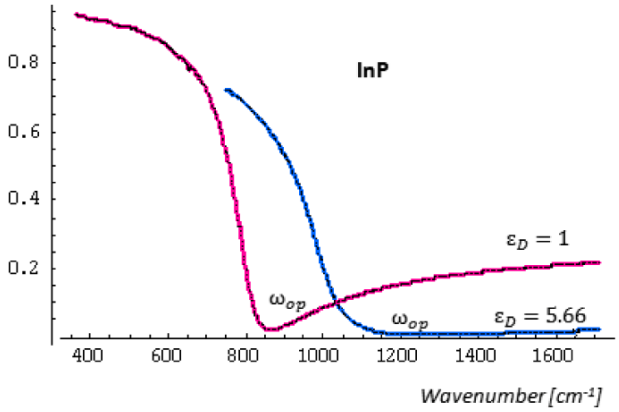

Fig. 3. Reflectivity spectrum of a heavily doped n-type InP: red curve – InP/air interface, blue curve – InP/diamond interface.

The GaAs and InP samples were pressed onto a diamond prism in the attenuated total reflection (ATR) configuration (GoldenGate ATR from Specac). The spectra are normalized using a diamond/vacuum reference measurement. In this configuration an air gap between the diamond and semiconductor sample exists. Figures 4 and 5 show the effect of the air gap thickness by the modeled ATR reflectivity. Comparing measured spectra presented in Fig. 2 and 3 with the modeled ATR reflectivity one determines the air gap thickness to be less than 50 nm and thus having a minute effect on the positions of the reflectivity minima.

#224420 - $15.00 USD Received 9 Oct 2014; revised 12 Dec 2014; accepted 21 Dec 2014; published 13 Jan 2015

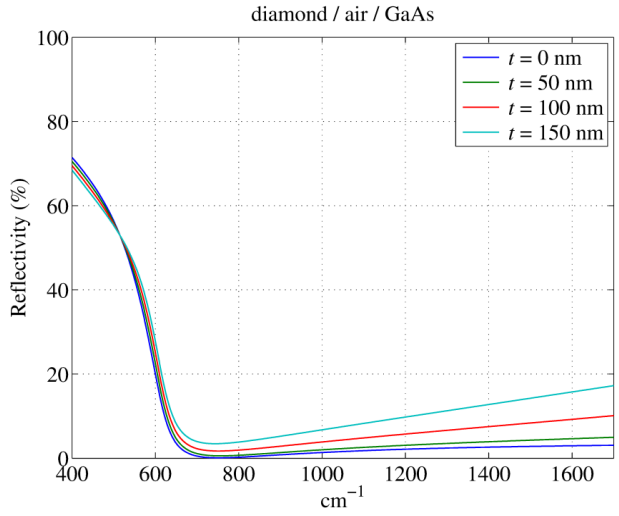

Fig. 4. Modeled effect of air gap thickness on diamond/GaAs ATR reflectivity.

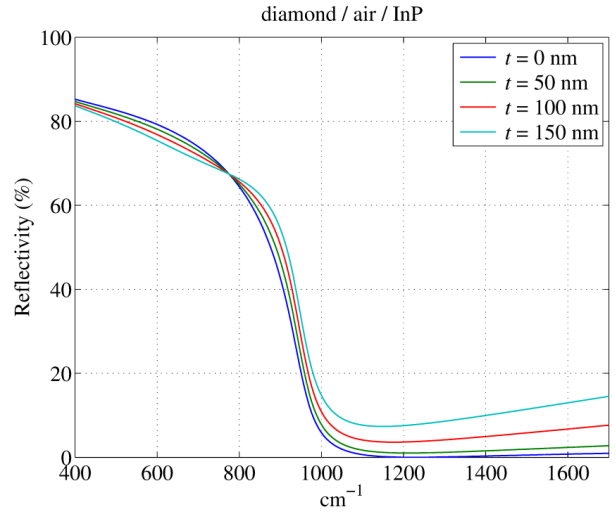

Fig. 5. Modeled effect of air gap thickness on diamond/InP ATR reflectivity.

Raman scattering

Raman scattering measurements used a Nicolet NXR 9650 FT-Raman spectrometer that employs a Nd:YVO_4 1064 nm laser and two detectors, a InGaAs and a Ge one. It covers a spectral range from 4000 cm^{-1} down to 50 cm^{-1} with a resolution of up to 1 cm^{-1}. Examples of the Raman scattering measurement of GaAs and InP samples are shown in Figs. 6 and 7, respectively. The scattering traces are normalized to unity and are shown as functions of the Raman shift. Two peaks are clearly seen in both cases. The narrower one at ω_- corresponds to the resonance frequency of the plasmon-LO phonon coupled mode below the TO phonon frequency, ω_{TO}, (i.e. the lower branch in figures below: Fig. 10 for GaAs and Fig. 11 for InP). The peak at ω_+ corresponds to the resonance frequency of the plasmon-LO phonon coupled mode above the LO phonon frequency, ω_{LO}, (i.e. the upper branch in figures below: Fig. 10 for GaAs and Fig. 11 for InP).

#224420 - $15.00 USD Received 9 Oct 2014; revised 12 Dec 2014; accepted 21 Dec 2014; published 13 Jan 2015

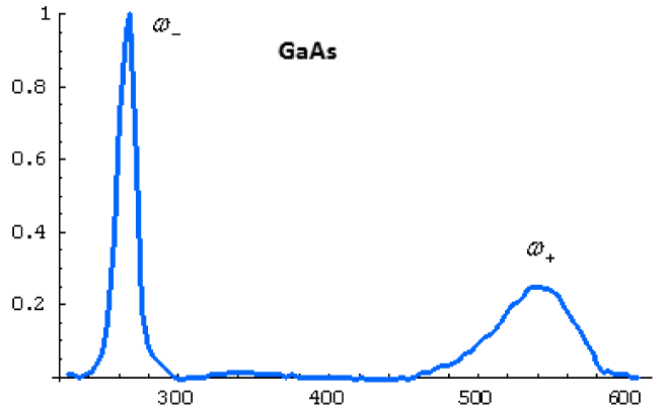

Fig. 6. Raman scattering trace of a heavily doped n-type GaAs.

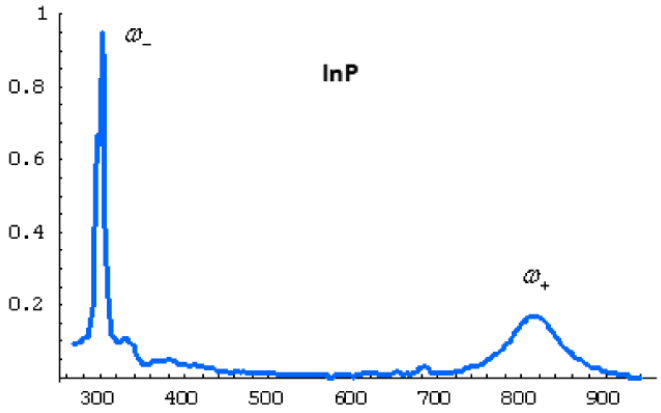

Fig. 7. Raman scattering trace of a heavily doped n-type InP.

Table 2 summarizes the measured values of the relevant parameters. Values of ω_{op} and R_{min} are for ε_D=1 (air).

Table 2. Measured parameters

Parameter/Material	GaAs	InP
plasma edge, $\omega_{op}\,[cm^{-1}]$	576	865
minimum reflectivity, R_{min}	0.043	0.022
plasmon-phonon energy, $\omega_-\,[cm^{-1}]$	267	304
plasmon-phonon energy, $\omega_+\,[cm^{-1}]$	547	812

4. Interpretation and discussion

Infrared reflectivity

The experimental air/semiconductor interface reflectivity data yielded the plasma energy edge values shown in Table 2. Expressed in wavelength, one obtains $\lambda_{op}^{GaAs}=17.36\,\mu m$ and $\lambda_{op}^{InP}=11.55\,\mu m$. The dispersive behavior of ε_S as described by Eq. (4) must be considered since the measurement wavelength is relatively close to the optical TO phonon resonance,

#224420 - $15.00 USD Received 9 Oct 2014; revised 12 Dec 2014; accepted 21 Dec 2014; published 13 Jan 2015

which lies at $\lambda_{TO} = 37.2\,\mu m$ for GaAs and at $\lambda_{TO} = 32.9\,\mu m$ for InP [19,20]. Figures 8 and 9, generated from Eq. (4), show the dispersion for GaAs and InP, respectively. The thin red vertical lines in both figures indicate the wavelength of the measurements. It is worth noting again that even high concentrations of free carriers in the studied samples have only a minute effect on the actual dispersion of ε_S. On the other hand, one has to use the dispersed value of ε_S when determining important semiconductor material parameters, i.e. the relaxation time, the effective mass and the mobility, from the measurements. Literature usually reports the use of ε_∞ instead of ε_S thus ignoring the dispersion of ε_S, which then yields results in error. An example in[11] referring to a difference between calculated and measured data of about 15% can be corrected down to about 5% by simply including the dispersive behavior of the permittivity.

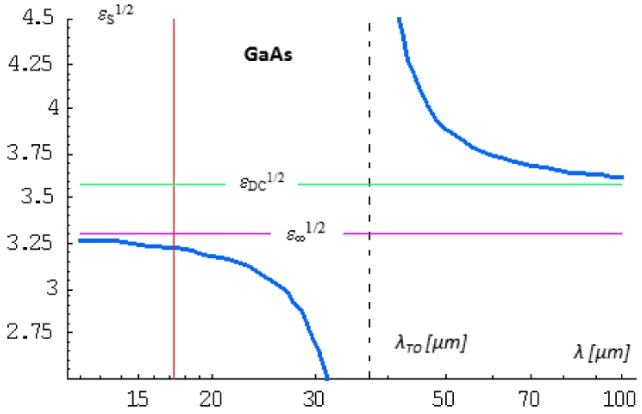

Fig. 8. Refractive index dispersion of GaAs: blue curve – material refractive index, thin red line – measured plasma edge.

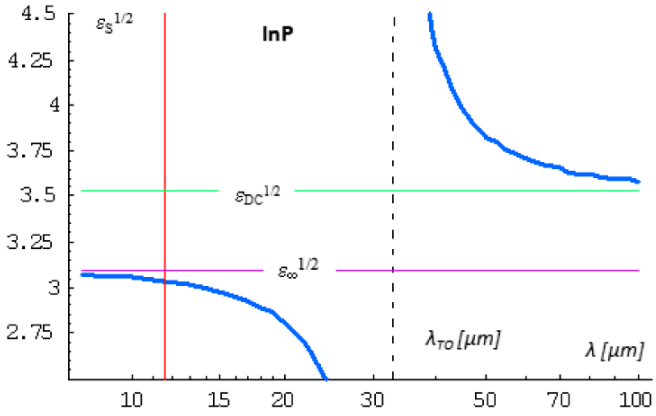

Fig. 9. Refractive index dispersion of InP: blue curve – material refractive index, thin red line – measured plasma edge.

Raman scattering

The experimental Raman scattering data yielded the Raman shift values shown in Table 2. Figures 10 and 11 show the behavior described by Eq. (7) for the GaAs and InP samples, respectively. The blue curve is the lower branch and the green curve is the upper branch of the plasmon-LO phonon coupled mode resonance frequency, respectively. The straight red

#224420 - $15.00 USD Received 9 Oct 2014; revised 12 Dec 2014; accepted 21 Dec 2014; published 13 Jan 2015

line represents the plasma frequency as defined in Eq. (5). The thin vertical line corresponds to the concentration of the respective samples measured.

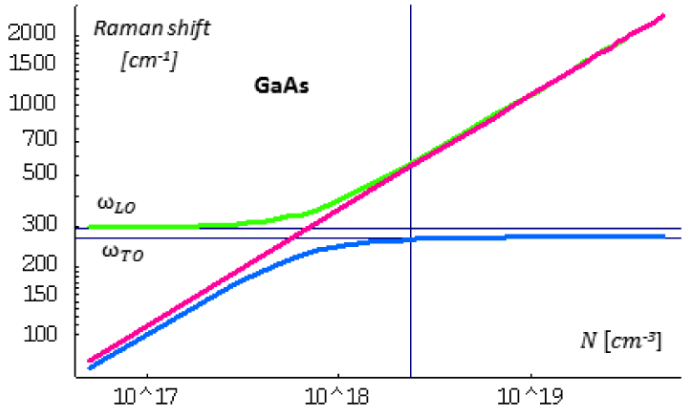

Fig. 10. Raman shift versus concentration for a heavily doped n-type GaAs: green curve – upper branch of coupled plasmon–LO phonon, red line – plasma frequency, blue curve – lower branch of coupled plasmon–LO phonon, thin vertical line – concentration of the sample studied.

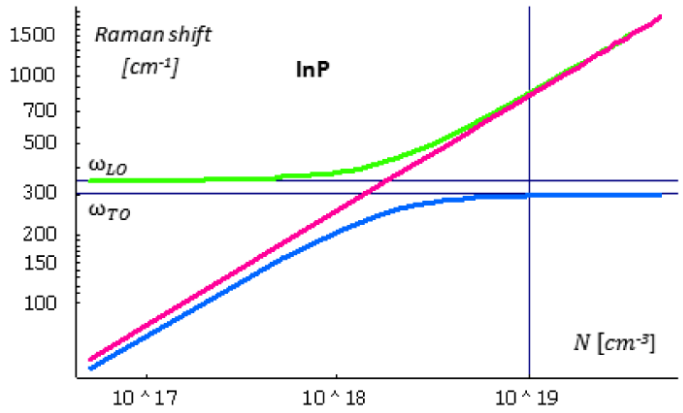

Fig. 11. Raman shift versus concentration for a heavily doped n-type InP: green curve – upper branch of coupled plasmon–LO phonon, red line – plasma frequency, blue curve – lower branch of coupled plasmon–LO phonon, thin vertical line – concentration of the sample studied.

The Figs. clearly indicate why the ω_- trace is distinguished in the measurements from the ω_+ trace. Figures also offer understanding why, in our case of samples with heavy doping, ω_- is practically identical with ω_{TO} while ω_+ practically yields ω_p directly since its trace is too close to the plasma frequency to be discerned.

Having now all the measured data (Table 2) along with the basic parameters (Table 1), one can exploit Eqs. (2)-(11) above to determine desired material parameters; namely the relaxation time, the effective mass, and the mobility. Table 3 summarizes all these parameters determined from the two independent measurements.

#224420 - $15.00 USD Received 9 Oct 2014; revised 12 Dec 2014; accepted 21 Dec 2014; published 13 Jan 2015

Table 3. Resulting material parameters

Parameter/Material	GaAs	InP
dispersed permittivity, ε_S	10.4	9.2
Drude frequency, $\tilde{\omega}_p\,[cm^{-1}]$	1753	2457
relaxation time, $\tau\,[fs]$	92	79
plasma frequency, $\omega_p\,[cm^{-1}]$	535	799
effective mass, m^*/m_0	0.07	0.147
mobility, $\mu\,[cm^2/V\cdot s]$	2338	951

Since it is known that heavy n-doping of semiconductors causes their effective mass to increase due to the non-parabolic band, and even double over just an order of magnitude increase in concentration [21], our results are in a good agreement with published values. As it is observed from the values of the effective mass, they are higher than usually used in literature [18], but mostly for undoped materials (0.063 and 0.08 for GaAs and InP, respectively), i.e. valid for the bottom of the conduction band. The electron scattering in degenerate semiconductors occurs mostly at the Fermi level and an appropriate effective mass m_F^* must be used.

The increase of the effective mass due to the band non-parabolicity and increasing Fermi level for GaAs can be described by an empirical formula [22] $m_{eff} = 0.064 + 1.26\times10^{-20}N - 4.37\times10^{-40}N^2$. An effective mass of 0.092, which is higher than the obtained one, is predicted by this approximate formula for the nominal concentration of $2.4\text{x}10^{18}$ cm^{-3}. On the other hand, the effective mass of 0.07 measured is estimated by the formula to be for a concentration of $4.8\text{x}10^{17}$ cm^{-3}.

In the case of InP the effective mass of 0.11 was obtained in [23] for a $1\text{x}10^{19}$ cm^{-3} doping concentration while the measured value of 0.147 can be expected for fourfold higher sulfur doping concentrations [14].

It should also be noted that the values in Table 3 obtained from the experimental values of both independent measurement methods are within less than 1% of each other. Therefore an excellent agreement has been obtained between measured data by two independent methods and the calculations from the models for both independent theoretical and experimental studies.

5. Conclusion

Interaction of light at an interface of a heavily doped n-type GaAs and InP, and a dielectric leading to a new plasmonic solution was exploited in an experimental determination of the plasma frequency, ω_p, the relaxation time, τ, the effective mass, m^*, and the mobility, μ. Two independent measurements, namely the infrared reflectivity and the Raman scattering, yielded three crucial parameters, i.e. the plasma edge frequency, ω_{op}, which corresponds to the new optical plasmon discovered previously, the reflectivity minimum, R_{min}, and the coupled plasmon-LO phonon frequency, ω_+, that sufficiently and accurately allow determining the above mentioned important semiconductor material parameters. The permittivity of a semiconductor was corrected from a simple Drude model to include background permittivity dispersion due to the vicinity of the transverse optical phonon (TO lattice vibrational mode). Free carrier absorption effects were also accounted for by including the damping factor in the model. Results are in a very good agreement with known data. Obtained accurate determination of the desired parameters from the two independent measurements in the demonstrated combined experimental and modelling approach suggests

#224420 - $15.00 USD Received 9 Oct 2014; revised 12 Dec 2014; accepted 21 Dec 2014; published 13 Jan 2015

that this method can be advantageously exploited as a new semiconductor material characterization technique.

Acknowledgment

This work was supported by Natural Sciences and Engineering Council of Canada (NSERC) and its Collaborative Research and Training Experience (CREATE) Advanced Science in Photonics and Innovative Research in Engineering (ASPIRE) Program, by IT4 Innovations Centre of Excellence project, reg. no. CZ.1.05/1.1.00/02.0070, by the Czech Republic grant (GACR) P205/11/2137, and by the New Creative Teams in Priorities of Scientific Research grant CZ1.07/2.3.00/30.0055. Authors acknowledge Raman measurements by M. Johnson and K. Hewitt of Dalhousie University, and data processing by J. Chochol of VŠB – Technical University of Ostrava.

#224420 - $15.00 USD Received 9 Oct 2014; revised 12 Dec 2014; accepted 21 Dec 2014; published 13 Jan 2015